Multicarrier Communication over Underwater Acoustic Channels with Nonuniform Doppler Shifts

Baosheng Li, *Student Member, IEEE*, Shengli Zhou, *Member, IEEE*, Milica Stojanovic, *Member, IEEE*, Lee Freitag, *Member, IEEE*, and Peter Willett, *Fellow, IEEE*

***Abstract*— Underwater acoustic (UWA) channels are wideband in nature due to the small ratio of the carrier frequency to the signal bandwidth, which introduces frequency-dependent Doppler shifts. In this paper, we treat the channel as having a common Doppler scaling factor on all propagation paths, and propose a two-step approach to mitigating the Doppler effect: (1) non-uniform Doppler compensation via resampling that converts a "wideband" problem into a "narrowband" problem; and (2) high-resolution uniform compensation of the residual Doppler. We focus on zero-padded OFDM to minimize the transmission power. Null subcarriers are used to facilitate Doppler compensation, and pilot subcarriers are used for channel estimation. The receiver is based on block-by-block processing, and does not rely on channel dependence across OFDM blocks; thus, it is suitable for fast-varying UWA channels. The data from two shallow water experiments near Woods Hole, MA, are used to demonstrate the receiver performance. Excellent performance results are obtained even when the transmitter and the receiver are moving at a relative speed of up to 10 knots, at which the Doppler shifts are greater than the OFDM subcarrier spacing. These results suggest that OFDM is a viable option for high-rate communications over wideband underwater acoustic channels with nonuniform Doppler shifts.**

***Index Terms*— Underwater acoustic communication, multicarrier modulation, OFDM, wideband channels.**

I. Introduction

Multicarrier modulation in the form of orthogonal frequency division multiplexing (OFDM) has prevailed in recent broadband wireless radio applications due to the low complexity of receivers required to deal with highly dispersive channels [2], [3]. This fact motivates the use of OFDM in underwater environments. Earlier works on OFDM focus mostly on conceptual system analysis and simulation based studies [4], [5], [6], [7], while experimental results are extremely scarce [8]–[12]. Recent investigations on underwater OFDM communication include [13] on non-coherent OFDM based on on-off-keying, [14] on a low-complexity adaptive OFDM receiver, and [15] on a pilot-tone based block-by-block receiver.

In this paper, we investigate the use of zero-padded OFDM [2], [16] for UWA communications. Zero-padding is used instead of cyclic prefix to save the transmission power spent on the guard interval. The performance of a conventional ZP-OFDM receiver is severely limited by the intercarrier interference (ICI) induced by fast channel variations within each OFDM symbol. Furthermore, the UWA channel is wideband in nature due to the small ratio of the carrier frequency to the signal bandwidth. The resulting frequency-dependent Doppler shifts render existing ICI reduction techniques ineffective. We treat the channel as having a common Doppler scaling factor on all propagation paths, and propose a two-step approach to mitigating the frequency-dependent Doppler shifts: (1) non-uniform Doppler compensation via resampling, which converts a "wideband" problem into a "narrowband" one; and (2) high-resolution uniform compensation of the residual Doppler for best ICI reduction.

The proposed practical receiver algorithms rely on the preamble and postamble of a packet consisting of multiple OFDM blocks to estimate the resampling factor, the null subcarriers to facilitate high-resolution residual Doppler compensation, and the pilot subcarriers for channel estimation. The receiver is based on block-by-block processing, and does not rely on channel coherence across OFDM blocks; thus, it is suitable for fast-varying underwater acoustic channels. To verify our approach, two experiments were conducted in shallow water: one in the Woods Hole Harbor, MA, on December 1, 2006, and the other in Buzzards Bay, MA, on December 15, 2006. Over a bandwidth of 12 kHz, the data rates are 7.0, 8.6, 9.7 kbps with QPSK modulation and rate 2/3 convolutional coding, when the numbers of subcarriers are 512, 1024, and 2048, respectively. Excellent performance is achieved for the latter experiment, while reasonable performance is achieved for the former experiment whose channel has a delay spread much larger than the guard interval. The receiver performs successfully even at a relative speed of up to 10 knots, resulting in Doppler shifts that are greater than the OFDM subcarrier spacing. These results suggest that OFDM is a viable option for high-rate UWA communications over underwater acoustic channels.

Manuscript received June 1, 2007 and revised September 14, 2007. B. Li and S. Zhou are supported by the ONR YIP grant N00014-07-1-0805 and the NSF grant ECCS-0725562. M. Stojanovic is supported by the ONR grant N00014-07-1-0202. L. Freitag is supported by the ONR grants N00014-02-6-0201 and N00014-07-1-0229. P. Willett is supported by the ONR grant N00014-07-1-0055. Part of this work was presented at the IEEE/MTS Oceans Conference, Aberdeen, Scotland, June 2007 [1]. The associate editor coordinating the review of this paper and approving it for publication was Prof. Urbashi Mitra.

B. Li, S. Zhou, and P. Willett are with Department of Electrical and Computer Engineering, University of Connecticut, Storrs, CT 06269 (email: baosheng@engr.uconn.edu; shengli@engr.uconn.edu; willett@engr.uconn.edu).

M. Stojanovic is with Massachusetts Institute of Technology, Cambridge, MA 02139 (email: millitsa@mit.edu).

L. Freitag is with the Woods Hole Oceanographic Institution, Woods Hole, MA 02543 (email: lfreitag@whoi.edu).

Publisher Item Identifier

The rest of the paper is organized as follows. In Section II, the performance of a conventional OFDM receiver is analyzed. In Section III, a two-step approach to mitigating the Doppler shifts is proposed, and the practical receiver algorithms are specified. In Sections IV and V the receiver performance is reported. Section VI contains the conclusions.

II. Zero-Padded OFDM for Underwater Acoustic Channels

Let T denote the OFDM symbol duration and T_g the guard interval. The total OFDM block duration is $T' = T + T_g$. The frequency spacing is $\Delta f = 1/T$. The kth subcarrier is at the frequency

$$f_k = f_c + k\Delta f, \quad k = -K/2, \ldots, K/2-1, \tag{1}$$

where f_c is the carrier frequency and K subcarriers are used so that the bandwidth is $B = K\Delta f$.

Let us consider one ZP-OFDM block. Let $d[k]$ denote the information symbol to be transmitted on the kth subcarrier. The non-overlapping sets of active subcarriers $\mathcal{S}_A$ and null subcarriers $\mathcal{S}_N$ satisfy $\mathcal{S}_A \cup \mathcal{S}_N = \{-K/2, \ldots, K/2-1\}$. The transmitted signal in passband is then given by

$$s(t) = \mathrm{Re}\left\{ \left[\sum_{k\in\mathcal{S}_\mathrm{A}} d[k] e^{j2\pi k\Delta f t} g(t) \right] e^{j2\pi f_c t} \right\}, \quad t \in [0, T+T_g], \tag{2}$$

where $g(t)$ describes the zero-padding operation, i.e., $g(t) = 1, t \in [0, T]$ and $g(t) = 0$ otherwise.

We consider a multipath underwater channel that has the impulse response

$$c(\tau, t) = \sum_p A_p(t)\delta(\tau - \tau_p(t)), \tag{3}$$

where $A_p(t)$ is the path amplitude and $\tau_p(t)$ is the time-varying path delay. To develop our receiver algorithms, we adopt the following assumptions.

A1) All paths have a similar Doppler scaling factor a such that

$$\tau_p(t) \approx \tau_p - at. \tag{4}$$

In general, different paths could have different Doppler scaling factors. The method proposed in this paper is based on the assumption that all the paths have the same Doppler scaling factor. When this is not the case, part of useful signals are treated as additive noise, which could increase the overall noise variance considerably. However, we find that as long as the dominant Doppler shift is caused by the direct transmitter/receiver motion, as it is the case in our experiments, this assumption seems to be justified.

A2) The path delays τ_p, the gains A_p, and the Doppler scaling factor a are constant over the block duration T'.

The OFDM block durations are $T = 42.67, 85.33, 170.67$ ms in our experiments when the numbers of subcarriers are 512, 1024, 2048, respectively. Assumption A2) is reasonable within these durations, as the channel coherence time is usually on the order of seconds.

The received signal in passband is then

$$\tilde{y}(t) = \mathrm{Re}\left\{ \sum_p A_p \left[\sum_{k\in\mathcal{S}_A} d[k] e^{j2\pi k\Delta f(t+at-\tau_p)} g(t+at-\tau_p) \right] \times e^{j2\pi f_c(t+at-\tau_p)} \right\} + \tilde{n}(t), \tag{5}$$

where $\tilde{n}(t)$ is the additive noise. The baseband version $y(t)$ of the received signal satisfies $\tilde{y}(t) = \mathrm{Re}\left\{y(t)e^{j2\pi f_c t}\right\}$, and can be written as

$$y(t) = \sum_{k\in\mathcal{S}_A} \left\{ d[k] e^{j2\pi k\Delta f t} e^{j2\pi a f_k t} \times \left[\sum_p A_p e^{-j2\pi f_k \tau_p} g(t+at-\tau_p) \right] \right\} + n(t), \tag{6}$$

where $n(t)$ is the additive noise in baseband. Based on the expression in (6), we observe two effects:

(i) the signal from each path is scaled in duration, from T to $T/(1+a)$;

(ii) each subcarrier experiences a Doppler-induced frequency shift $e^{j2\pi a f_k t}$, which depends on the frequency of the subcarrier. Since the bandwidth of the OFDM signal is comparable to the center frequency, the Doppler-induced frequency shifts on different OFDM subcarriers differ considerably; i.e., the narrowband assumption does not hold.

The frequency-dependent Doppler shifts introduce strong intercarrier interference if an effective Doppler compensation scheme is not performed prior OFDM demodulation.

III. Receiver Design

We first present in Section III-A the technical approach to mitigating the frequency-dependent Doppler shifts, and then specify in Section III-B practical receiver algorithms that we apply to the experimental data.

A. A Two-Step Approach to Mitigating the Doppler Effect

We propose a two-step approach to mitigating the frequency-dependent Doppler shifts due to fast-varying underwater acoustic channels:

1. Non-uniform Doppler compensation via resampling. This step converts a “wideband” problem into a “narrowband” problem.
2. High-resolution uniform compensation of residual Doppler. This step fine-tunes the residual Doppler shift corresponding to the “narrowband” model for best ICI reduction.

The resampling methodology has been shown effective to handle the time-scale change in underwater communications, see e.g., [17], [18]. Resampling can be performed either in passband or in baseband. For convenience, let us present these

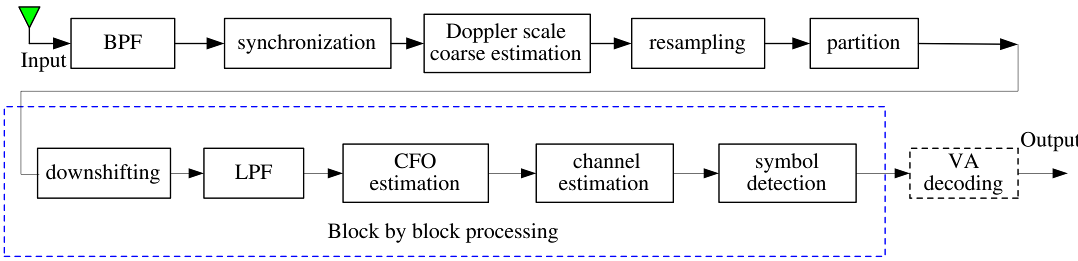

Fig. 1. The detailed receiver diagram on one receive-element.

steps using passband signals. In the first step, we resample the received waveform $\tilde{y}(t)$ using a resampling factor b:

$$\tilde{z}(t) = \tilde{y}\left(\frac{t}{1+b}\right). \tag{7}$$

Resampling has two effects: (1) it rescales the waveform, and (2) it introduces a frequency-dependent Doppler compensation. With $\tilde{y}(t)$ from (5) and $\tilde{z}(t) = \text{Re}\{z(t)e^{j2\pi f_c t}\}$, the baseband signal $z(t)$ is

$$z(t) = e^{j2\pi \frac{a-b}{1+b} f_c t} \sum_{k\in\mathcal{S}_A} \Bigg\{ d[k] e^{j2\pi k\Delta f \frac{1+a}{1+b} t} \times \left[\sum_p A_p e^{-j2\pi f_k \tau_p} g\left(\frac{1+a}{1+b}t - \tau_p\right)\right]\Bigg\} + v(t), \tag{8}$$

where $v(t)$ is the additive noise. The target is to make $\frac{1+a}{1+b}$ as close to one as possible. With this in mind, we have

$$z(t) \approx e^{j2\pi \frac{a-b}{1+b} f_c t} \sum_{k\in\mathcal{S}_A} \Bigg\{ d[k] e^{j2\pi k\Delta f t} \times \left[\sum_p A_p e^{-j2\pi f_k \tau_p} g(t - \tau_p)\right]\Bigg\} + v(t). \tag{9}$$

The residual Doppler effect can be viewed as the same for all subcarriers. Hence, a wideband OFDM system is converted into a narrowband OFDM system with a frequency-independent Doppler shift

$$\epsilon = \frac{a-b}{1+b} f_c. \tag{10}$$

In radio applications, a carrier frequency offset (CFO) between the transmitter and the receiver leads to an expression of the received signal in the form (9) [19], [20]. For this reason, we call the term ϵ in (10) as CFO when a narrowband model is concerned.

Compensating for the CFO in $z(t)$, we obtain

$$e^{-j2\pi\epsilon t} z(t) \approx \sum_{k\in\mathcal{S}_A} \Bigg\{ d[k] e^{j2\pi k\Delta f t} \times \left[\sum_p A_p e^{-j2\pi f_k \tau_p} g(t - \tau_p)\right]\Bigg\} + e^{-j2\pi\epsilon t} v(t), \tag{11}$$

where the subcarriers stay orthogonal. On the output of the demodulator in the m-th subchannel, we have [2], [16].

$$\begin{aligned} z_m &= \frac{1}{T}\int_0^{T_g+T} e^{-j2\pi\epsilon t} z(t) e^{-j2\pi m\Delta f t} dt \\ &\approx C(f_m) d[m] + v_m, \end{aligned} \tag{12}$$

where $C(f) := \sum_p A_p e^{-j2\pi f \tau_p}$ and v_m is the resulting noise. Hence, ICI-free reception is approximately achieved. Rescaling and phase-rotation of the received signal thus restore the orthogonality of the subcarriers of ZP-OFDM. The correlation in (12) can be performed by *overlap-adding* of the received signal, followed by FFT processing [2], [16].

In practice, the scale factor b and the CFO ϵ need to be determined from the received data. They can be estimated either separately or jointly. Note that each estimate of b will be associated with a resampling operation, which is costly. It is desirable to limit the number of resampling operations to as few as possible. At the same time, high-resolution algorithms are needed to fine-tune the CFO term ϵ for best ICI reduction.

We next specify the practical algorithms that we apply to the experimental data.

B. Practical Receiver Algorithms

The received signal is directly sampled and all processing is performed on discrete-time entries. Fig. 1 depicts the receiver processing for each element, where BPF, LPF, and VA stand for bandpass filtering, low-pass filtering, and Viterbi algorithm, respectively. Next, we discuss several key steps.

1) Doppler scaling factor estimation: Coarse estimation of the Doppler scaling factor is based on the preamble and the postamble of a data packet. (This idea was used in e.g., [17] for single carrier transmissions.) The packet structure, containing N_b OFDM blocks, is shown in Fig. 2. By cross-correlating the received signal with the known preamble and postamble, the receiver estimates the time duration of a packet, $\hat{T}_{\rm rx}$. The time duration of this packet at the transmitter side is $T_{\rm tr}$. By comparing $\hat{T}_{\rm rx}$ with $T_{\rm tx}$, the receiver infers how the received signal has been compressed or dilated by the channel:

$$\hat{T}_{\rm rx} = \frac{T_{\rm tx}}{1+\hat{a}} \quad \Rightarrow \quad \hat{a} = \frac{T_{\rm tx}}{\hat{T}_{\rm rx}} - 1. \tag{13}$$

The receiver then resamples the packet with a resampling factor $b = \hat{a}$ used in (7). We use the polyphase-interpolation based resampling method available in Matlab.

Fig. 2. Packet structure.

2) CFO estimation: A CFO estimate is generated for each OFDM block within a packet. We use null subcarriers to facilitate estimation of the CFO. We collect $K+L$ samples after resampling for each OFDM block into a vector[1] $\mathbf{z} = [z(0), \ldots, z(K+L-1)]^T$, assuming that the channel has $L+1$ taps in discrete time. The channel length can be inferred based on the synchronization output of the preamble, and its estimation does not need to be very accurate. We define a $(K+L)\times 1$ vector $\mathbf{f}_m = [1, e^{j2\pi m/K}, \ldots, e^{j2\pi m(K+L-1)/K}]^T$, and a $(K+L)\times(K+L)$ diagonal matrix $\mathbf{\Gamma}(\epsilon) = \text{diag}(1, e^{j2\pi T_c \epsilon}, \cdots, e^{j2\pi T_c(K+L-1)\epsilon})$, where $T_c = T/K$ is the time interval for each sample. The energy of the null subcarriers is used as the cost function

$$J(\epsilon) = \sum_{m\in\mathcal{S}_N} |\mathbf{f}_m^{\mathcal{H}} \mathbf{\Gamma}^{\mathcal{H}}(\epsilon)\mathbf{z}|^2. \qquad (14)$$

If the receiver compensates the data samples with the correct CFO, the null subcarriers will not see the ICI spilled over from neighboring data subcarriers. Hence, an estimate of ϵ can be found through

$$\hat{\epsilon} = \arg\min_{\epsilon} J(\epsilon), \qquad (15)$$

which can be solved via one-dimensional search for ϵ. This high-resolution algorithm corresponds to the MUSIC-like algorithm proposed in [19] for cyclic-prefixed OFDM.

Instead of the one-dimensional search, one can also use the standard gradient method as in [20] or a bi-sectional search. A coarse-grid search is needed to avoid local minima before the gradient method or the bi-sectional search is applied [21].

Remark 1: The null subcarriers can also facilitate joint resampling and CFO estimation. This approach corresponds to a two-dimensional search: when the scaling factor b and the CFO ϵ are correct, the least signal spill-over into null subcarriers is observed. However, the computational complexity is high for a two-dimensional search. This algorithm can be used if no coarse estimate of the Doppler scaling factor (e.g., from the pre- and post-amble of a packet) is available.

3) Pilot-tone based channel estimation: After resampling and CFO compensation, the ICI induced by CFO is greatly reduced. Due to assumption A2, we will not consider the ICI due to channel variations within each OFDM block. Note that ICI analysis and suppression in the presence of fast-varying channels have been treated extensively in the literature, see e.g., the references listed in [22, Ch. 19]. Ignoring ICI, the signal in the mth subchannel can be represented as [c.f. (12)]

$$z_m = \mathbf{f}_m^{\mathcal{H}} \mathbf{\Gamma}^{\mathcal{H}}(\hat{\epsilon})\mathbf{z} = H(m)d[m] + v_m, \qquad (16)$$

[1]Bold upper case and lower case letters denote matrices and column vectors, respectively; $(\cdot)^T$, $(\cdot)^*$, and $(\cdot)^{\mathcal{H}}$ denote transpose, conjugate, and Hermitian transpose, respectively.

where $H(m) = C(f_m)$ is the channel frequency response at the mth subcarrier and v_m is the additive noise. On a multipath channel, the coefficient $H(m)$ can be related to the equivalent discrete-time baseband channel parameterized by $L+1$ complex-valued coefficients $\{h_l\}_{l=0}^{L}$ through

$$H(m) = \sum_{l=0}^{L} h_l e^{-j2\pi lm/K}. \qquad (17)$$

To estimate the channel frequency response, we use K_p pilot tones at subcarrier indices $p_1, \ldots, p_{K_p}$; i.e., $\{d[p_i]\}_{i=1}^{K_p}$ are known to the receiver.

As long as $K_p \geq L+1$, we can find the channel taps based on a least-squares formulation

$$\underbrace{\begin{bmatrix} z_{p_1} \\ \vdots \\ z_{p_{K_p}} \end{bmatrix}}_{:=\mathbf{z}_p} = \begin{bmatrix} v_{p_1} \\ \vdots \\ v_{p_{K_p}} \end{bmatrix} + \underbrace{\begin{bmatrix} d[p_1] & & \\ & \ddots & \\ & & d[p_{K_p}] \end{bmatrix}}_{:=\mathbf{D}_s} \times \underbrace{\begin{bmatrix} 1 & e^{-j\frac{2\pi}{K}p_1} & \cdots & e^{-j\frac{2\pi}{K}p_1 L} \\ \vdots & \vdots & \ddots & \vdots \\ 1 & e^{-j\frac{2\pi}{K}p_{K_p}} & \cdots & e^{-j\frac{2\pi}{K}p_{K_p} L} \end{bmatrix}}_{:=\mathbf{V}} \underbrace{\begin{bmatrix} h_0 \\ \vdots \\ h_L \end{bmatrix}}_{:=\mathbf{h}}. \qquad (18)$$

To minimize the complexity, we will adhere to the following two design rules:

d1) The K_p pilot symbols are equally spaced within K subcarriers;

d2) The pilot symbols are PSK signals with unit amplitude.

Since the pilots are equi-spaced, we have that $\mathbf{V}^{\mathcal{H}}\mathbf{V} = K_p \mathbf{I}_{L+1}$ [23], and since they are of unit-amplitude, we have that $\mathbf{D}_s^{\mathcal{H}}\mathbf{D}_s = \mathbf{I}_{K_p}$. Therefore, the LS solution for (18) simplifies to

$$\hat{\mathbf{h}}_{\text{LS}} = \frac{1}{K_p}\mathbf{V}^{\mathcal{H}}\mathbf{D}_s^{\mathcal{H}}\mathbf{z}_p. \qquad (19)$$

This solution does not involve matrix inversion, and can be implemented by an K_p-point IFFT. With the time-domain channel estimate $\hat{\mathbf{h}}_{\text{LS}}$, we obtain the frequency domain estimates using the expression (17).

4) Multi-channel combining: Multi-channel reception greatly improves the system performance through diversity; see e.g., [24] on multi-channel combining for single-carrier transmissions over UWA channels. In an OFDM system, multi-channel combining can be easily performed on each subcarrier. Suppose that we have N_r receive elements, and let z_m^r, $H^r(m)$, and v_m^r denote the output, the channel

TABLE I

INPUT DATA STRUCTURE AND THE CORRESPONDING BIT RATES

K	# of active subcarriers (K_a)	# of null subcarriers (K_n)	# of blocks in a packet (N_b)	bit rates without coding $\frac{2(K_a-K/4)}{(T+T_g)}$	bit rates after rate 2/3 channel coding
512	484	28	64	10.52 kbps	7.0 kbps
1024	968	56	32	12.90 kbps	8.6 kbps
2048	1936	112	16	14.55 kbps	9.7 kbps

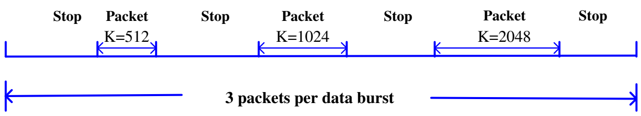

Fig. 3. Each data burst consists of three packets, with $K = 512$, $K = 1024$, and $K = 2048$, respectively

frequency response, and the additive noise observed at the mth subcarrier of the rth element. We thus have:

$$\underbrace{\begin{bmatrix} z_m^1 \\ \vdots \\ z_m^{N_r} \end{bmatrix}}_{:=\mathbf{z}_m} = \underbrace{\begin{bmatrix} H^1(m) \\ \vdots \\ H^{N_r}(m) \end{bmatrix}}_{:=\tilde{\mathbf{h}}_m} d[m] + \underbrace{\begin{bmatrix} v_m^1 \\ \vdots \\ v_m^{N_r} \end{bmatrix}}_{:=\mathbf{v}_m}. \tag{20}$$

Assuming that $\mathbf{v}_m$ has independent and identically distributed entries, the optimal maximum-ratio combining (MRC) yields

$$\hat{d}[m] = \left(\tilde{\mathbf{h}}_m^{\mathcal{H}} \tilde{\mathbf{h}}_m\right)^{-1} \tilde{\mathbf{h}}_m^{\mathcal{H}} \mathbf{z}_m. \tag{21}$$

Doppler scaling factor, CFO, and channel estimation are performed independently on each receiving element according to the procedure described in Sections III-B.1 to III-B.3. An estimate of the channel vector $\tilde{\mathbf{h}}_m$ is then formed, and used to obtain the data symbol estimates in (21).

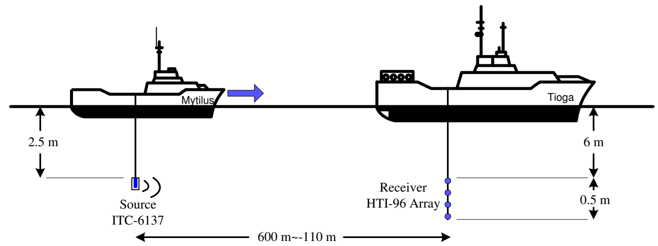

Fig. 4. The configuration of the experiment in Buzzards Bay.

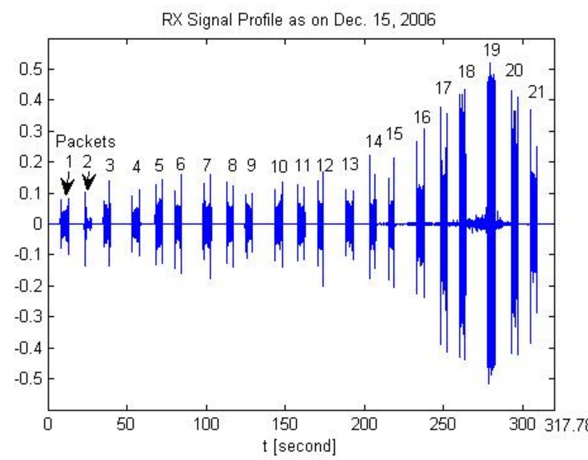

Fig. 5. The received signal (amplitude) for the Buzzards Bay experiment.

IV. Performance Results for the Experiment in Buzzards Bay

The bandwidth of the OFDM signal is $B = 12$ kHz, and the carrier frequency is $f_c = 27$ kHz. The transmitted signal thus occupies the frequency band between 21 kHz and 33 kHz. We use zero-padded OFDM with a guard interval of $T_g = 25$ ms per OFDM block. The respective number of subcarriers used in the experiment is $K = 512$, 1024, and 2048. The subcarrier spacing is $\Delta f = 23.44$ Hz, 11.72 Hz, and 5.86 Hz, and the OFDM block duration is $T = 1/\Delta f = 42.67$ ms, 85.33 ms, and 170.67 ms. We use rate 2/3 convolutional coding, obtained by puncturing a rate 1/2 code with the generator polynomial (23,35). Coding is applied within the data stream for each OFDM block. QPSK modulation is used. For $K = 512, 1024, 2048$, each packet contains $N_b = 64, 32, 16$ OFDM blocks, respectively. The total number of information bits per packet is 30976. The signal parameters and the corresponding data rates are summarized in Table I, where the overhead of null subcarriers and $K_p = K/4$ pilot subcarriers is accounted for.

Fig. 3 depicts one data burst that consists of three packets with $K = 512$, $K = 1024$, and $K = 2048$, respectively. During the experiments, the same data burst was transmitted multiple times while the transmitter was on the move.

The WHOI acoustic communication group conducted the experiment on Dec. 15, 2006 in Buzzards Bay, MA. The transmitter was located at a depth of about 2.5 meters and the receiver consisted of a four-element vertical array of length 0.5 m submerged at a depth of about 6 meters. The transmitter was mounted on the arm of the vessel Mytilus, and the receiver array was mounted on the arm of the vessel Tioga. OFDM signals were transmitted while Mytilus was moving towards Tioga, starting at 600 m away, passing by Tioga, and ending at about 100 m away. The experiment configuration is shown in Fig. 4.

The received signal was directly A/D converted. The signal received on one element is shown in Fig. 5, which contains 7 data bursts or 21 packets. The following observations can be made from Fig. 5.

1) The received power is increasing before packet 19, and decreasing thereafter.
   This observation is consistent with the fact that Mytilus passed Tioga around that time.
2) A sudden increase in noise shows up around packet 19.

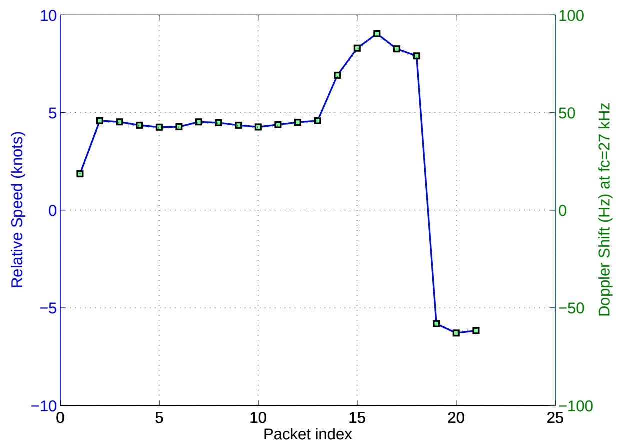

Fig. 6. Coarse estimation of the relative speed and the Doppler shift at $f_c = 27$ kHz for element 1.

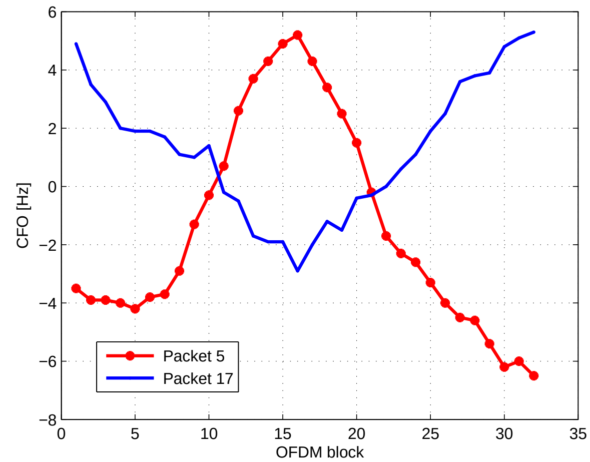

Fig. 7. The estimated residual Doppler (CFO) for packet 5 (with an estimated speed of 4.25 knots) and packet 17 (with an estimated speed of 8.26 knots). The CFO fluctuates rapidly from one block to another.

This noise comes from the Mytilus when it was very close to Tioga.

3) The second packet was severely distorted. The reason is unclear.

Simple data processing reveals the following:

4) The signals prior to packet 19 were compressed, which agrees with the fact that the transmitter was moving towards the receiver. The signals after that were dilated, confirming the fact that the transmitter was moving away from the receiver.

We next present numerical results based on the sequence of the receiver processing shown in Fig. 1. We present a selected set of results and comparisons.

A. Doppler scaling factor estimation

For each of the 21 packets transmitted, the algorithm of Section III-B.1 was used to estimate the Doppler scaling factor. Based on each Doppler scaling factor $\hat{a}$, the relative speed between the transmitter and the receiver was estimated as $\hat{v} = \hat{a} \cdot c$, using a nominal sound speed of $c = 1500$ m/s. The relative speed and the resulting Doppler shift at the carrier frequency, $\hat{a}f_c$, are shown in Fig. 6, which summarizes the results for element 1.

We see from Fig. 6 that the Doppler shifts are much larger than the OFDM subcarrier spacing. For example, if $\hat{v} = 8.30$ knots (packet 15), which indicates that Mytilus was moving toward Tioga at such a speed, the Doppler shift is 76.98 Hz at $f_c = 27$ kHz, while the subcarrier spacing is only $\Delta f = 23.44$ Hz, 11.72 Hz, and 5.86 Hz for $K = 512, 1024, 2048$, respectively. Hence, re-scaling the waveform (even coarsely) is necessary to mitigate the Doppler effect *nonuniformly* in the frequency domain.

B. High-resolution residual Doppler estimation

The high-resolution CFO estimation was performed on a block-by-block basis, as detailed in Section III-B.2. Fig. 7 shows the CFO estimates for packets 5 and 17 for $K = 1024$. We observe that the CFO changes from block to block roughly

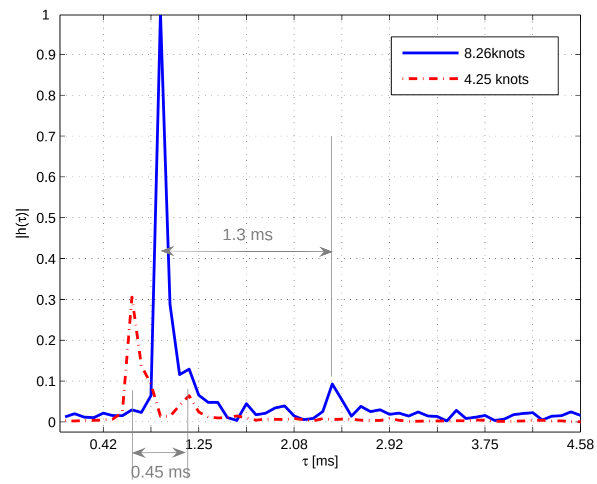

Fig. 8. Channel estimates for two example cases. One is for a case with an estimated speed of 4.25 knots (packet 5), the other is for a case with an estimated speed of 8.26 knots (packet 17). The channel delay spread is about 4.5 ms. There is a strong direct path between the transmitter and the receiver. The channel energy in the 8.26 knots case is higher than that in the 4.25 knots case, as the transmitter is closer. The second peak is conjectured to be from the bottom bounce.

continuously but cannot be regarded as constant. The CFO estimate is on the order of half of the subcarrier spacing. Without the CFO fine tuning, the receiver performance would deteriorate considerably.

We have also examined joint Doppler scaling factor and CFO fine tuning on each OFDM block based on null subcarriers, which requires a two-dimensional search for the scale b and the CFO ϵ. The performance improvement is marginal in this experiment, so we skip the results on the joint approach.

C. Channel estimation

Channel estimation is based on equi-spaced pilots, as detailed in Section III-B.3. Here we use $K_p = K/4$ pilot subcarriers. Fig. 8 depicts the estimated channel impulse responses for two cases. In one case Mytilus was moving toward Tioga at an estimated speed of 4.25 knots (packet 5),

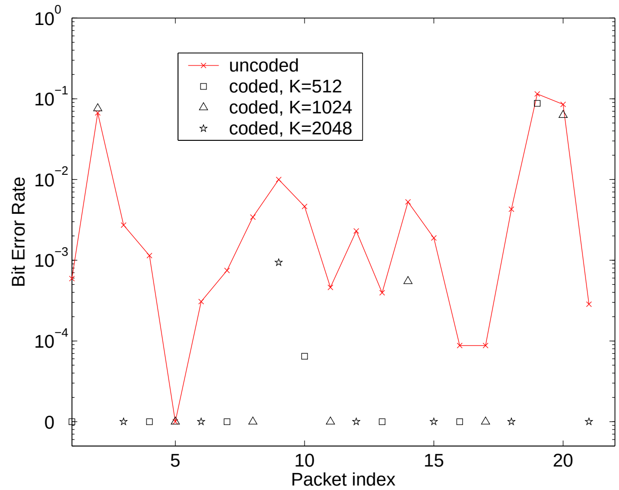

Fig. 9. The BERs averaged over each packet, element 1. Packets 10 and 19 (with $K = 512$) have decoding errors. Packets 2, 14, and 20 (with $K = 1024$) have decoding errors. Packet 9 (with $K = 2048$) has decoding errors.

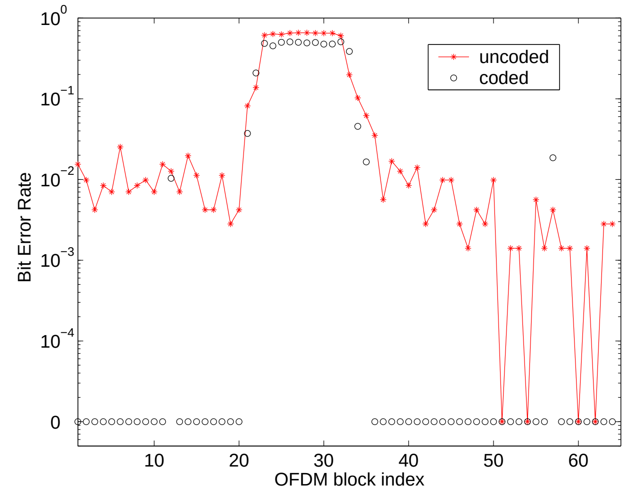

Fig. 10. The BERs averaged over each OFDM block, packet 19, $K = 512$, element 1.

and in the other case at an estimated speed of 8.26 knots (packet 17). The channel duration is about 4.5 ms. There is a strong direct path between the transmitter and the receiver. The energy in the 8.26 knots case is higher than that in the 4.25 knots case. This observation matches the power profile shown in Fig. 5.

A second path is also observed in Fig. 8. We conjecture that this path is from the bottom bounce. This conjecture is supported by a rough computation based on the channel geometry:

- Case 1: suppose that the distance is 400m, the depth is 12 m, then the delay between the bottom bounce and the direct path is $(2 \cdot \sqrt{200^2 + 12^2} - 400)/1500 = 0.48$ ms.
- Case 2: suppose that the transmitter is now 150m from the receiver, and the depth is 12m. Then the delay between the bottom bounce and the direct path is $(2 \cdot \sqrt{75^2 + 12^2} - 150)/1500 = 1.3$ ms.

These numbers roughly correspond to the inter-arrival times marked in Fig. 8. The arrival corresponding to the second peak can thus be assumed to be from a bottom bounce.

D. BER performance

We now report the BER performance without coding and with coding. The Viterbi algorithm was used for channel decoding.

We first plot the BER averaged over each packet in Fig. 9, for *one receiver* (element 1). In total, 6 out of 21 packets have errors after channel decoding. We now look into the BERs for each OFDM block inside the packets with decoding errors. The results are as follows.

- Packet 2 has 22 out of 32 blocks in error after decoding. This received packet was badly distorted, as can be seen in Fig. 5.
- Packet 9 has 4 out of 16 blocks ($K = 2048$) in error after decoding. Packet 10 has 2 out of 64 blocks ($K = 512$) in error after decoding. Packets 14 and 20 have 5 out of 32 block ($K = 1024$) in error each, after decoding. Except packet 20 having four consecutive blocks in error at the end, the error blocks for other packets are sporadic.
- It is interesting to look at packet 19, which has 17 out of 64 blocks in error after decoding. The BERs on the block level are shown in Fig. 10. The major portion of the error blocks occurred when the transmitter was passing by the receiver. As we observe from Fig. 5, the Doppler frequencies were changing from positive to negative values around packet 19, and the noise level increased considerably during the passing.
  We emphasize that with block-by-block processing, decoding errors in previous blocks have no impact on future blocks, as confirmed by Fig. 10.

We now report on the BER performance with *two receivers* (using elements 1 and 2). In total, there are four packets in error as follows. Packet 2 has 17 out of 32 blocks in error, packet 9 has 1 out of 16 blocks in error, packet 19 has 14 out of 64 blocks in error, and packet 20 has 4 out of 32 blocks in error. The sporadic block errors with single-receiver processing are mostly corrected with two-receiver processing. The BER plots are omitted due to space limitations.

For a real system, the block errors could be corrected via auto-repeat request (ARQ) procedures, or via coding strategies such as rateless coding [25, Chapter 50] that can effectively handle lost blocks.

V. Performance Results for the Experiment in Woods Hole Harbor

This experiment was conducted on Dec. 1, 2006. The same signal set as described in Section IV was used. The signal was transmitted from a depth of about 2.5 meters and received by a four-element vertical array with inter-element spacing 0.5 m, submerged at a depth of about 6 meters. The transmitter was mounted on the arm of the Mytilus, and the receiver array was attached to a buoy close to the dock. OFDM signals were transmitted while Mytilus was moving away from the dock starting from a distance of 50 m and ending at about 800 m.

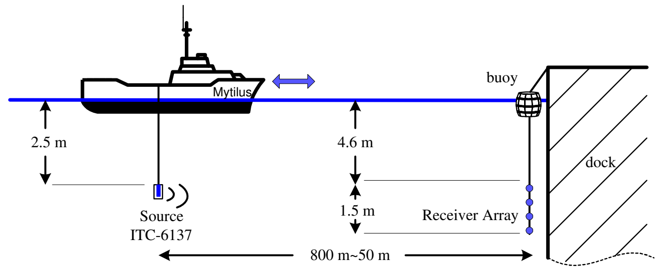

Fig. 11. The configuration for the experiment in Woods Hole harbor.

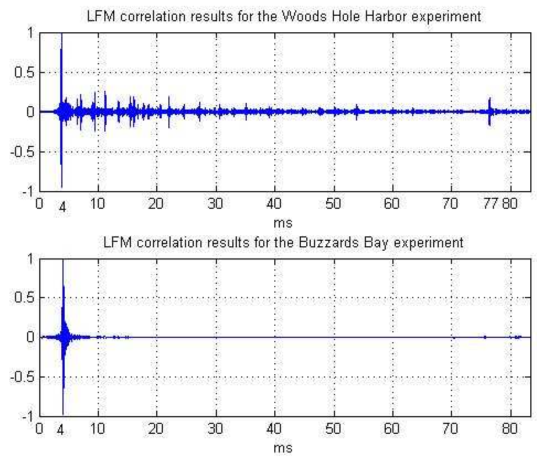

Fig. 12. The channel response estimates obtained by the linear frequency-modulated (LFM) preamble matching. The channel in the Woods Hole Harbor experiment has strong returns even after the guard interval of 25ms. As a result, inter-block interference exists. Unlike this situation, the channel in the Buzzards Bay experiment has delay spread much less than the guard interval.

Then Mytilus moved towards the dock. The configuration is shown in Fig. 11.

The channel condition was very difficult with strong multi-path after the guard interval of 25 ms. The last strong path is evident at about 80 ms, as shown in Fig. 12. This long delay spread is likely due to the reflections off the pilings near the dock.

With the channel delay spread longer than the guard interval, inter-block interference (IBI) emerges. We have not tried the channel shortening approach to reduce the IBI before OFDM demodulation (e.g., using methods from [26]–[28]). Instead, we treated all multipath returns after the guard interval as additive noise; hence, the system is operating at low signal-to-noise ratio (SNR). Nevertheless, with channel coding and multichannel reception, reasonable performance is still achieved, which speaks for the robustness of the receiver.

To illustrate the performance, we present results of two data bursts. One data burst was transmitted when Mytilus was moving away from the dock at a low speed of about 3 knots. The other data burst was transmitted when Mytilus was moving towards the dock at a high speed of about 10 knots.

A. Doppler scaling factor estimation

Table II shows the estimated speeds, which reflect the experimental settings. The Doppler shifts at $f_c = 27$ kHz are

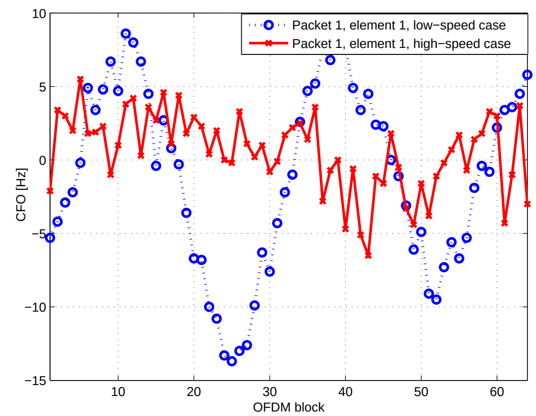

Fig. 13. The estimated residual Doppler shift of packet 1. $K = 512$ and each packet has 64 OFDM blocks.

very large for both cases. In the low-speed case, the Doppler shift is on the order of the OFDM subcarrier spacing (23.44 Hz when $K = 512$). In the high-speed case, the Doppler shift is much greater than the subcarrier spacing.

B. High-resolution Residual Doppler estimation

Figs. 13, 14, and 15 show the CFO estimates for packets 1, 2 and 3 of element 1, respectively. The following observations are made:

1) The CFO changes from block to block smoothly, but cannot be regarded as constant.
2) The residual CFO effect cannot be neglected.
3) The CFO estimates are on the order of half of the subcarrier spacings for the low speed case.
4) In the low-speed case, the CFO changes periodically over time. The period is the same for all three settings. In the high-speed case, this phenomenon is not present. A possible explanation for this effect is that Mytilus rises and falls due to waves, which is more pronounced at low speed than at high speed.
5) Note that fewer null subcarriers are available in the $K = 512$ case than the $K = 1024$ and $K = 2048$ cases, and hence the CFO estimation is more affected by the noise realizations. When K increases, more null subcarriers lead to better noise averaging, and the corresponding curves look smoother. This trend is clearly shown in Figs. 13, 14, and 15.

C. Channel estimation

Figs. 16 and 17 depict the channel estimates for the 3-knot and the 10-knot cases, respectively. We observe several stable paths whose delays do not depend on the location and the speed of the transmitter. For example, there is one stable path around 3 ms. This path could be best interpreted as the first reflected path from the dock. The receiver is about 2 meters from the dock. Hence, the dock-reflected path will be delayed by $2 \cdot 2/1500 = 2.6$ ms relative to the direct path. This is a constant delay, which does not depend on the distance between the transmitter and the receiver.

TABLE II
COARSE ESTIMATION OF DOPPLER SHIFT AND RELATIVE SPEED FOR ELEMENT 1.

The low speed case			The high speed case		
Packet	Doppler shift due to scaling at f_c (Hz)	Relative speed (knots)	Packet	Doppler shift due to scaling at f_c (Hz)	Relative speed (knots)
1 (K=512)	-23.84	-2.56	1 (K=512)	91.49	9.86
2 (K=1024)	-21.30	-2.29	2 (K=1024)	87.88	9.47
3 (K=2048)	-24.06	-2.60	3 (K=2048)	96.03	10.36

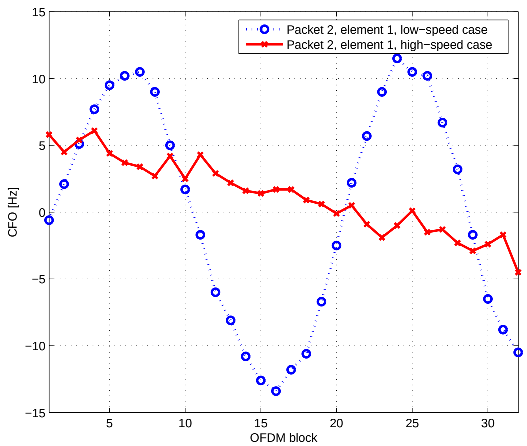

Fig. 14. The estimated residual Doppler of packet 2. $K = 1024$ and each packet has 32 OFDM blocks.

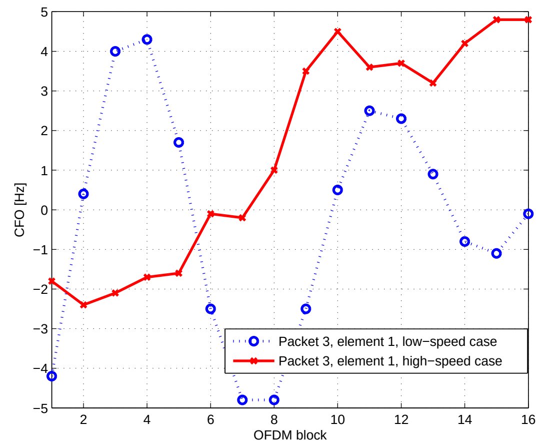

Fig. 15. The estimated residual Doppler of packet 3. $K = 2048$ and each packet has 16 OFDM blocks.

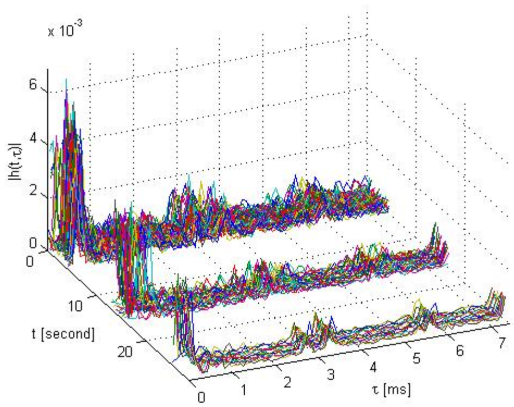

Fig. 16. The estimated channel impulse responses (magnitude) for packets 1-3; element 1 in the low speed case.

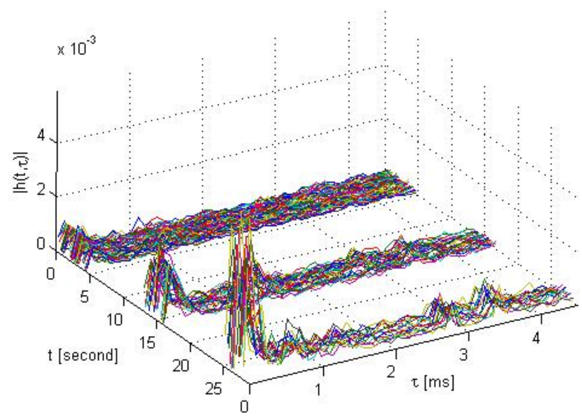

Fig. 17. The estimated channel impulse responses (magnitude) for packets 1-3; element 1 in the high speed case.

D. BER performance

Since the channel condition was particularly severe in this test, both coding (rate 2/3) and multi-channel combining were necessary to improve the BER performance. The following performance results are obtained with three receiving-elements.

For packet 3 with $K = 2048$, Figs. 18 and 19 compare the uncoded performance and the coded performance on the OFDM block level, with single channel or multichannel reception, in different settings. With MRC, the uncoded BERs averaged over the packet are $2 \cdot 10^{-2}$ and $1.7 \cdot 10^{-2}$ for the low speed and high speed cases, respectively. After rate 2/3 coding, the BERs averaged over the packet are $1.6 \cdot 10^{-3}$ and $5.8 \cdot 10^{-3}$ for the low speed and high speed cases, respectively. We observe the following from Figs. 18 and 19.

1) The uncoded BER is large, on the order of 10^{-1} for single-element reception and 10^{-2} for multi-channel reception.
2) For single-element reception with large uncoded BER, coding does not help. However, for multi-channel reception, the BER performance is much improved when coding is used.

With $K = 1024$, the BERs averaged over the packet (packet #2) after MRC and coding is $1.1 \cdot 10^{-2}$ and $6.5 \cdot 10^{-2}$ for the

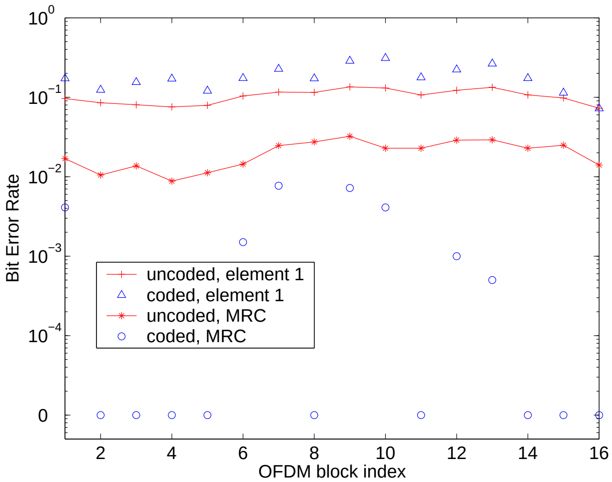

Fig. 18. The BERs for each OFDM block, the low speed case, $K = 2048$.

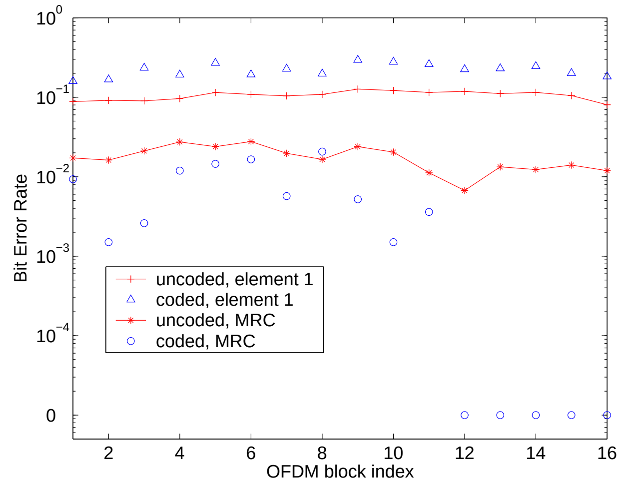

Fig. 19. The BERs for each OFDM block, the high speed case, $K = 2048$.

low and high speed cases, respectively. With $K = 512$, the BER averaged over the packet (packet #1) after MRC and coding is $3 \cdot 10^{-2}$ for the low speed case, while the receiver does not work well for the high speed case. These results show that the setting with larger K has better performance in this experiment. When K increases, the effect of channel variation within one OFDM block becomes more severe, while on the other hand, the receiver has more null subcarriers and pilot subcarriers for better CFO and channel estimation against noise [c.f. Table I]. Note that the sampling rate is fixed for all three cases, and, hence, the discrete-time channel has approximately the same number of taps. The noise effect outweighs the channel-variation effect in this data set, since the receiver operates at a noise-limited region, due to the large noise contributed by the arrivals after the guard interval.

Although the results for the Woods Hole harbor experiment are worse than those for the Buzzards Bay experiment, they demonstrate the robustness of the proposed receiver in the presence of a difficult channel with a delay spread much larger than the OFDM guard interval. Note that a 16-state rate 2/3 code is used here. A much stronger channel code (e.g. the nonbinary low-density-parity-check (LDPC) code used in [29]) would considerably improve the BER performance.

VI. Conclusions

In this paper we investigated the application of OFDM in wideband underwater acoustic channels with nonuniform Doppler shifts. To compensate for the non-uniform Doppler distortion, a two-step approach was used: resampling followed by high-resolution uniform compensation of the residual Doppler. Null subcarriers facilitate Doppler compensation, and pilot subcarriers are used for channel estimation. The receiver is based on block-by-block processing, and, hence, it is suitable for fast-varying channels.

The method proposed was tested in two shallow water experiments. Over a bandwidth of 12 kHz, the data rates are 7.0, 8.6, 9.7 kbps with QPSK modulation and rate 2/3 convolutional coding, when the number of subcarriers are 512, 1024, and 2048, respectively. Good performance was achieved even when the transmitter and the receiver were moving at a relative speed of up to 10 knots, where the Doppler shifts are greater than the OFDM subcarrier spacing. Experimental results suggest that OFDM is a viable candidate for high-rate transmission over underwater acoustic channels.

Future research will address several topics, including shortening methods for channels whose delay spread is longer than the guard interval, extension of resampling to generalized time-varying filtering for channels with different Doppler scaling factors on different paths, and multi-input multi-output (MIMO) techniques [29]–[31].

Acknowledgements

We thank the reviewers for their thoughtful comments.

References

[1] B. Li, S. Zhou, M. Stojanovic, L. Freitag, and P. Willett, “Non-uniform Doppler compensation for zero-padded OFDM over fast-varying underwater acoustic channels,” in *Proc. of MTS/IEEE OCEANS conference*, Aberdeen, Scotland, June 18-21, 2007.

[2] Z. Wang and G. B. Giannakis, “Wireless multicarrier communications: Where Fourier meets Shannon,” *IEEE Signal Processing Magazine*, vol. 17, no. 3, pp. 29–48, May 2000.

[3] R. Prasad, *OFDM for Wireless Communications Systems*. Artech House Publishers, 2004.

[4] E. Bejjani and J. C. Belfiore, “Multicarrier coherent communications for the underwater acoustic channel,” in *Proc. of OCEANS*, 1996.

[5] W. K. Lam and R. F. Ormondroyd, “A coherent COFDM modulation system for a time-varying frequency-selective underwater acoustic channel,” in *Proc. of the 7th International Conference on Electronic Engineering in Oceanography*, June 1997, pp. 198–203.

[6] W. K. Lam, R. F. Ormondroyd, and J. J. Davies, “A frequency domain adaptive coded decision feedback equalizer for a broadband UWA COFDM system,” in *Proc. of OCEANS*, 1998.

[7] Y. V. Zakharov and V. P. Kodanev, “Multipath-Doppler diversity of OFDM signals in an underwater acoustic channel,” in *IEEE International Conference on Acoustics, Speech, and Signal Processing*, vol. 5, June 2000, pp. 2941–2944.

[8] S. Coatelan and A. Glavieux, “Design and test of a coded OFDM system on the shallow water acoustic channel,” in *Proc. of OCEANS*, Sept. 1994.

[9] B. Kim and I. Lu, “Sea trial results of a robust and spectral-efficient OFDM underwater communication system (Abstract),” *The Journal of the Acoustical Society of America*, vol. 109, no. 5, pp. 2477–2477, May 1, 2001.

[10] R. Bradbeer, E. Law, and L. F. Yeung, "Using multi-frequency modulation in a modem for the transmission of near-realtime video in an underwater environment," in *Proc. of IEEE International Conference on Consumer Electronics*, June 2003.

[11] P. J. Gendron and T. C. Yang, "Environmental and motion effects on orthogonal frequency division multiplexed on-off keying," in *American Institute of Physics Conference Series*, vol. 728, Nov. 2004, pp. 98–105.

[12] M. Chitre, S. H. Ong, and J. Potter, "Performance of coded OFDM in very shallow water channels and snapping shrimp noise," in *Proceedings of MTS/IEEE OCEANS*, vol. 2, 2005, pp. 996–1001.

[13] P. J. Gendron, "Orthogonal frequency division multiplexing with on-off-keying: Noncoherent performance bounds, receiver design and experimental results," *U.S. Navy Journal of Underwater Acoustics*, vol. 56, no. 2, pp. 267–300, Apr. 2006.

[14] M. Stojanovic, "Low complexity OFDM detector for underwater channels," in *Proc. of MTS/IEEE OCEANS conference*, Boston, MA, Sept. 18-21, 2006.

[15] B. Li, S. Zhou, M. Stojanovic, and L. Freitag, "Pilot-tone based ZP-OFDM demodulation for an underwater acoustic channel," in *Proc. of MTS/IEEE OCEANS conference*, Boston, MA, Sept. 18-21, 2006.

[16] B. Muquet, Z. Wang, G. B. Giannakis, M. de Courville, and P. Duhamel, "Cyclic prefix or zero-padding for multi-carrier transmissions?" *IEEE Transactions on Communications*, vol. 50, no. 12, pp. 2136–2148, Dec. 2002.

[17] B. S. Sharif, J. Neasham, O. R. Hinton, and A. E. Adams, "A computationally efficient Doppler compensation system for underwater acoustic communications," *IEEE Journal of Oceanic Engineering*, vol. 25, no. 1, pp. 52–61, Jan. 2000.

[18] P. Beaujean and L. R. LeBlanc, "Adaptive array processing for high-speed acoustic communication in shallow water," *IEEE Journal of Oceanic Engineering*, vol. 29, no. 3, pp. 807–823, July 2004.

[19] U. Tureli and H. Liu, "A high-efficiency carrier estimator for OFDM communications," *IEEE Communications Letters*, vol. 2, no. 4, pp. 104–106, Apr. 1998.

[20] X. Ma, C. Tepedelenlioglu, G. B. Giannakis, and S. Barbarossa, "Non-data-aided carrier offset estimations for OFDM with null subcarriers: Identifiability, algorithms, and performance," *IEEE Journal on Selected Areas in Communications*, vol. 19, no. 12, pp. 2504–2515, Dec. 2001.

[21] H. Yan, S. Zhou, Z. Shi, and B. Li, "A DSP implementation of OFDM acoustic modem," in *Proc. of the ACM International Workshop on UnderWater Networks (WUWNet)*, Montréal, Québec, Canada, September 14, 2007.

[22] A. F. Molisch, *Wireless Communications*. John Wiley & Sons, LTD, 2005.

[23] J. Rinne and M. Renfors, "Pilot spacing in orthogonal frequency division multiplexing systems on practical channels," *IEEE Transactions on Consumer Electronics*, vol. 42, no. 4, pp. 959–962, Nov. 1996.

[24] M. Stojanovic, J. A. Catipovic, and J. G. Proakis, "Adaptive multichannel combining and equalization for underwater acoustic communications," *Journal of the Acoustical Society of America*, vol. 94, no. 3, pp. 1621–1631, 1993.

[25] D. MacKay, *Information Theory, Inference, and Learning Algorithms*. Cambridge University Press, 2003.

[26] R. K. Martin and C. R. Johnson, Jr., "Adaptive equalization: transitioning from single-carrier to multicarrier systems," *IEEE Signal Processing Magazine*, vol. 22, no. 6, pp. 108–122, Nov. 2005.

[27] J. Kleider and X. Ma, "Adaptive channel shortening equalization for coherent OFDM doubly selective channels," in *Proc. of International Conference on Acoustics, Speech, and Signal Processing*, Toulouse, France, May 15-19, 2006.

[28] X. Ma, R. J. Baxley, J. Kleider, and G. T. Zhou, "Superimposed training for channel shortening equalization in OFDM," in *Proc. of Milcom*, Oct. 2006.

[29] B. Li, S. Zhou, M. Stojanovic, L. Freitag, J. Huang, and P. Willett, "MIMO-OFDM over an underwater acoustic channel," in *Proc. of MTS/IEEE OCEANS conference*, Vancouver, BC, Canada, Sept. 29 - Oct. 4, 2007.

[30] D. B. Kilfoyle, J. C. Preisig, and A. B. Baggeroer, "Spatial modulation experiments in the underwater acoustic channel," *IEEE Journal of Oceanic Engineering*, vol. 30, no. 2, pp. 406–415, Apr. 2005.

[31] S. Roy, T. M. Duman, V. McDonald, and J. G. Proakis, "High rate communication for underwater acoustic channels using multiple transmitters and space-time coding: Receiver structures and experimental results," *IEEE Journal of Oceanic Engineering*, 2008 (to appear).

PLACE PHOTO HERE

Baosheng Li (S'05) received the B.S. and the M.S. degrees in the electronic and communications engineering from the Harbin Institute of Technology, Harbin, China, in 2002 and 2004, respectively. He is currently working toward the Ph.D. degree in the Department of Electrical and Computer Engineering, University of Connecticut, Storrs.

His research interests lie in the areas of communications and signal processing, currently focusing on multi-transceiver and multi-carrier modulation algorithms for underwater acoustic communications.

PLACE PHOTO HERE

Shengli Zhou (M'03) received the B.S. degree in 1995 and the M.Sc. degree in 1998, from the University of Science and Technology of China (USTC), Hefei, both in electrical engineering and information science. He received his Ph.D. degree in electrical engineering from the University of Minnesota (UMN), Minneapolis, in 2002. He has been an assistant professor with the Department of Electrical and Computer Engineering at the University of Connecticut (UCONN), Storrs, since 2003.

His general research interests lie in the areas of wireless communications and signal processing. His recent focus has been on underwater acoustic communications and networking. He served as an Associate Editor for the IEEE TRANSACTIONS ON WIRELESS COMMUNICATIONS from February 2005 to January 2007. He received the ONR Young Investigator award in 2007.

PLACE PHOTO HERE

Milica Stojanovic (M'93) graduated from the University of Belgrade, Serbia, in 1988, and received the M.S. and Ph.D. degrees in electrical engineering from Northeastern University, Boston, MA, in 1991 and 1993. She is currently a principal scientist at the Massachusetts Institute of Technology, and also a guest investigator at the Woods Hole Oceanographic Institution.

Her research interests include digital communications theory and statistical signal processing, and their applications to mobile radio and underwater acoustic communication systems.

PLACE PHOTO HERE

Lee Freitag (M'88) holds BS and MS degrees in Electrical Engineering from the University of Alaska, Fairbanks, which he received in 1986 and 1987 respectively. He is currently a Senior Engineer at the Woods Hole Oceanographic Institution where he has worked on projects related to underwater acoustics for 15 years.

His research programs focus on underwater acoustic communication and navigation with a strong focus on UUVs, sensors and submarine systems. He is a member of IEEE and MTS.

PLACE PHOTO HERE

Peter Willett (F'03) received his BASc (Engineering Science) from the University of Toronto in 1982, and his PhD degree from Princeton University in 1986. He has been a faculty member at the University of Connecticut ever since, and since 1998 has been a Professor. His primary areas of research have been statistical signal processing, detection, machine learning, data fusion and tracking. He has interests in and has published in the areas of change/abnormality detection, optical pattern recognition, communications and industrial/security condition monitoring.

He is editor-in-chief for IEEE Transactions on Aerospace and Electronic Systems, and until recently was associate editor for three active journals: IEEE Transactions on Aerospace and Electronic Systems (for Data Fusion and Target Tracking) and IEEE Transactions on Systems, Man, and Cybernetics, parts A and B. He is also associate editor for the IEEE AES Magazine, editor of the AES Magazines periodic Tutorial issues, associate editor for ISIFs electronic Journal of Advances in Information Fusion, and is a member of the editorial board of IEEEs Signal Processing Magazine. He has been a member of the IEEE AESS Board of Governors since 2003. He was General Co-Chair (with Stefano Coraluppi) for the 2006 ISIF/IEEE Fusion Conference in Florence, Italy, Program Co-Chair (with Eugene Santos) for the 2003 IEEE Conference on Systems, Man, and Cybernetics in Washington DC, and Program Co-Chair (with Pramod Varshney) for the 1999 Fusion Conference in Sunnyvale.